PCCP

PAPER

View Article Online
View Journal | View Issue

Cite this: *Phys. Chem. Chem. Phys.*, 2018, **20**, 7265

Excitation spectra of retinal by multiconfiguration pair-density functional theory†

Sijia S. Dong, Laura Gagliardi * and Donald G. Truhlar *

Received 27th October 2017,
Accepted 8th February 2018

DOI: 10.1039/c7cp07275a

rsc.li/pccp

Retinal is the chromophore in proteins responsible for vision. The absorption maximum of retinal is sensitive to mutations of the protein. However, it is not easy to predict the absorption spectrum of retinal accurately, and questions remain even after intensive investigation. Retinal poses a challenge for Kohn–Sham density functional theory (KS-DFT) because of the charge transfer character in its excitations, and it poses a challenge for wave function theory because the large size of the molecule makes multiconfigurational perturbation theory methods expensive. In this study, we demonstrate that multiconfiguration pair-density functional theory (MC-PDFT) provides an efficient way to predict the vertical excitation energies of 11-*Z* retinal, and it reproduces the experimentally determined absorption band widths and peak positions better than complete active space second-order perturbation theory (CASPT2). The consistency between complete active space self-consistent field (CASSCF) and KS-DFT dipole moments is demonstrated to be a useful criterion in selecting the active space. We also found that the nature of the terminal groups and the conformations of retinal play a significant role in the absorption spectrum. By considering a thermal distribution of conformations, we predict an absorption spectrum of retinal that is consistent with the experimental gas-phase spectrum. The location of the absorption peak and the spectral broadening based on MC-PDFT calculations agree better with experiments than those of CASPT2.

1. Introduction

The retinal molecule has been an important prototype target of photochemistry research for decades.[1–13] It is covalently bound to a type of protein, opsins, which are responsible for vision. The retinal ligand undergoes *cis–trans* isomerization upon light absorption, which triggers conformational changes in the opsin protein from the ''inactive state'' to the ''active state''. The activated opsin is involved in signal transduction in cells, which is eventually transformed into visual signals in brains.

Mutations in only a few amino acids in opsin can cause the wavelengths at which the retinal ligand absorbs most strongly to be different, and this is the basis of color vision.[14] The absorption spectrum of retinal may be sensitive to its conformations and/or its electrostatic environment.[15–17] Furthermore, the isomerization mechanism of retinal is still under debate after years of exploration. To study these problems, the first step is to describe the ground state and the excited states of retinal in the gas phase accurately and efficiently.

Kohn–Sham (KS) density functional theory (DFT) has difficulty in describing retinal correctly, especially for functionals without nonlocal exchange.[18] This is because photoisomerization of retinal involves excitations with some charge transfer (CT) character. Multireference perturbation theory methods such as complete active space second-order perturbation theory (CASPT2)[19] are generally more reliable than KS-DFT with most available approximate density functionals for charge transfer excitations, but CASPT2 is much more computationally expensive. Due to this expense and the size of the retinal molecule, it is infeasible to map the ground- and excited-state potential energy surfaces using CASPT2 without truncating the molecule to a simplified model. Multistate CASPT2[20] (MS-CASPT2) describes the potential energy surfaces better than state-specific CASPT2 when the mixing of states is strong, but it is even more expensive. Recently, we have developed the multiconfiguration pair-density functional theory (MC-PDFT)[21,22] method to overcome these kinds of challenges. MC-PDFT combines multiconfiguration wave function theory (WFT) with DFT. We obtain a reference wave function from a multiconfiguration WFT calculation, such as the multiconfiguration self-consistent field (MCSCF) method, and we calculate the electronic kinetic energy and classical electrostatic energy from the reference wave function. The other energy contributions are calculated from a density functional that is a functional of the

Department of Chemistry, Chemical Theory Center, and Minnesota Supercomputing Institute, University of Minnesota, Minneapolis, MN 55455, USA.
E-mail: truhlar@umn.edu, gagliard@umn.edu

† Electronic supplementary information (ESI) available. See DOI: 10.1039/c7cp07275a

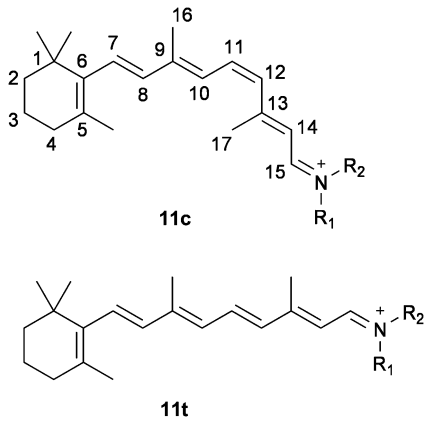

Fig. 1 Chemical structures of **11c** and **11t**.

total density and on-top pair density arising from the reference wave function.

Here, we compare the performance of MC-PDFT to that of linear response (LR) time-dependent density functional theory (TDDFT),[23] complete active space self-consistent field theory (CASSCF),[24] CASPT2, and MS-CASPT2 for describing the intramolecular charge transfer excitations of two large chromophores, namely 11-*Z-cis*-retinal (to be abbreviated as **11c**) and 11-*Z-trans*-retinal (**11t**). In native rhodopsin, it is the photoisomerization of **11c** to **11t** that triggers the activation of the protein. The structures of these molecules are shown in Fig. 1. Various terminal groups may be considered in the general case, and **11c** and **11t** refer to the general cases, with various terminal groups. However, in our calculations, in order to match the terminal groups to those in experimental measurements we want to compare to,[25] we consider **11c** with $R_1 = R_2 = CH_3$ (which is the positively charged 11-*cis*-dimethyl Schiff base and will be called **11c-dimethyl**) and **11t** with $R_1 = H$ and $R_2 = n$-butyl (which is the all-*trans n*-butyl protonated Schiff-base retinal and will be called **11t-butyl**).

2. Computational methods

To obtain the geometries used to compute vertical excitation energies, we first scanned the torsion angles for **11c-dimethyl**. Table 1 reports a list of initial guesses for torsion angles. After each initial conformation is generated based on Table 1, we optimized the conformation for **11c-dimethyl** using the M06-2X[26] density functional with the 6-31+G(d,p) basis set. We selected the M06-2X functional because it has been shown to generate reliable ground-state geometries of retinal analogs for studying their vertical excitations.[18,27] We did not rescan the torsion angles for **11t-butyl**; we assumed it would have similar torsion angles as **11c-dimethyl** if we only look at the lowest-energy conformations, excluding the terminal alkyl chain. For example, the rotation of the β-ionone ring in the *trans*-retinal has been found[27,28] to have a triple-well-shaped potential energy profile similar to *cis*-retinal in our study (Fig. S1 in the ESI†) and in that of Send and Sundhoolm.[29] Therefore, to obtain the lowest-energy conformations for **11t-butyl**, we took the three lowest energy conformations of **11c-dimethyl** and modified them into **11t-butyl** with the fully extended *n*-butyl group, and reoptimized their conformations. The Cartesian coordinates of each molecular geometry for which we computed the vertical excitation energies are included in the ESI.†

Table 1 Dihedral angle scanning range of **11c-dimethyl**. The atom numbers correspond to the labels in Fig. 1

Dihedral angle	Name	Range
C5═C6–C7═C8	θ_6	0–340° in 20° increments
C7═C8–C9═C10	θ_8	0, 180°
C9═C10–C11═C12	θ_{10}	0, 180°
C11═C12–C13═C14	θ_{12}	0, 180°
C13═C14–C15═C16	θ_{14}	0, 180°

All KS-DFT and LR-TDDFT calculations were carried out using *Gaussian 09*.[30] The *MSTor*[31,32] program was used to scan the torsional degrees of freedom of **11c-dimethyl**. All CASSCF, CASPT2, MS-CASPT2, and MC-PDFT calculations were carried out in *Molcas 8.2*.[33]

In this article, when the conformation is not specified in the discussion of vertical excitation energies, oscillator strengths, and dipole moments of a specific molecule, it means we are referring to the conformation with the lowest electronic energy (which will be labeled conformation s0048 in Section 3.3 below). Where not otherwise noted, the basis set TZVP[34,35] was employed; the basis sets def2-SVP,[36,37] def2-SVPD,[36–38] def2-TZVP,[36,37] ma-SVP,[39] and ma-TZVP[39] were also tested and are discussed briefly in later sections.

For both **11c** and **11t**, we did state-averaged CASSCF (SA-CASSCF) over the 3 lowest states. The guess orbitals for the CASSCF calculations were either the Hartree–Fock (HF) orbitals or the orbitals from another CASSCF calculation. The two-electron integrals were Cholesky decomposed to a threshold of 10^{-4}. We carried out the CASPT2 calculations with an imaginary shift of 0.1 Hartree, which is the value recommended for *Molcas*, and a standard IPEA shift of 0.25 Hartree, which is the default in *Molcas*.

As discussed in detail in later sections, the active spaces were selected based on whether the dipole moments calculated for the various states are consistent with TDDFT calculations. Dipole moments of charged species are origin dependent. For the dipole moment calculations of each molecular geometry, we used the same coordinates for CASSCF and TDDFT calculations (the coordinates in the ESI†), and we used the origin of the coordinate system as the origin (except where noted otherwise in the ESI†). Comparing Table 2 with Table S10 of the ESI,† we see that the dipole moments calculated using the two origin choices differ by at most 0.54 D, which is much smaller than the differences from using different active spaces, and Table S10 (ESI†) shows that using the center of nuclear charges as the origin does not change our conclusions based on dipole moments.

When comparing results from different multiconfigurational methods for a given active space of a given molecule using a given basis set, the same reference wave function was used for CASPT2 as for MC-PDFT. The CASPT2 oscillator strengths were computed using CASSCF transition dipole

Table 2 Dipole moments of **11c-dimethyl** (in debye) calculated using CASSCF with different active spaces and calculated using KS-DFT (S_0) and TDDFT (S_1 and S_2). The solution for the CASSCF(10,10) calculation using CASSCF(8,8) or HF orbitals as the guess orbitals is labeled #1, and the solution for the CASSCF(10,10) calculation using CASSCF(12,12) orbitals as the guess orbitals is labeled #2

	S_0	S_1	S_2
(4,4)	16.35	13.65	13.06
(6,6)	15.27	6.20	1.90
(8,8)	20.39	7.67	18.29
(10,10) #1	16.45	10.75	9.60
(10,10) #2	18.35	2.79	4.05
(12,12)	24.12	6.73	23.22
M06-2X	16.89	10.16	8.17
M06-HF	18.70	10.42	8.57
CAM-B3LYP	16.55	10.14	8.01
PBE0	15.70	9.60	9.75

moments extracted from the *RASSI* program of *Molcas 8.2* combined with CASPT2 energy values, and the MC-PDFT oscillator strengths were computed using the same transition dipole moments and MC-PDFT energy values.

The MC-PDFT vertical excitation energies discussed in this article were obtained with the tPBE[22,40] on-top density functional. Results from other on-top density functionals, in particular, ftPBE,[40,41] tBLYP,[22,42,43] ftBLYP,[41–43] trevPBE,[22,44] ftrevPBE,[41,44] tLSDA,[22,45–47] and ftLSDA,[41,45–47] typically differ by $\sim$0.05 eV or less. This is demonstrated in Table S3 of the ESI.† Therefore, we focus our discussion on the tPBE results.

Simulated spectra were generated using the second-order Franck–Condon displaced harmonic oscillator (FC-DHO) model as implemented in *FCBand*.[48] For these calculations, vertical excitation energies and oscillator strengths were taken from the corresponding CASPT2 or MC-PDFT calculations, ground-state vibrational frequencies were from DFT calculations, and the gradients of the excited states were from TDDFT calculations. The DFT and TDDFT calculations were performed with the M06-2X density functional and the 6-31+G(d,p) basis set. To consider the thermal distribution of conformations in the spectra, we calculated the Gibbs free energy of the most stable conformations within 3 kcal mol^{-1} electronic energy of the lowest-energy conformation with a frequency scaling factor of 0.967.[49] Then, the weight of each conformation in the spectra was calculated based on a Boltzmann distribution. This procedure was carried out for 298.15 K, 500 K, and 700 K, respectively. The 298.15 K results will be shown and discussed in the article, and the higher-temperature results are reported in the ESI.†

3. Results and discussion

3.1. Active space selection

A crucial part of a multiconfiguration calculation is to determine the active space. The active spaces are designated by (ne, nl), where ne is the number of active electrons, and nl is the number of active orbitals. When studying conjugated π systems, one systematic approach would be to include all the π electrons and π orbitals in the active space; this would yield (12,12) active spaces for **11c** and **11t**. However, we found that this is not the best choice for retinal, as explained later in this section. In particular, our analysis on **11c** and studies by others[27] both indicate that the energy of retinal has two or three minima as the dihedral angle θ_6 (which corresponds to C5═C6–C7═C8; see Table 1) is rotated, with the global minimum at $\theta_6 = -40^\circ$ (as obtained with the M06-2X functional in this work) or at -68° (as obtained by the CASSCF method by Valsson and Fillippi[27]). This means that the two π electrons on the β-ionone ring are not fully conjugated with the other π electrons in the lowest-energy structure. It is well known that one can obtain unphysical results with multireference methods if one uses an unbalanced active space; it might be unbalanced to include some non-conjugated orbitals when we do not include a balanced subset of the non-conjugated orbitals, for example, all carbon–carbon bond orbitals, which would be prohibitively expensive. In addition, although including the full valence π system in the active space seems to be a common choice for polyenes, in some previous retinal studies, a smaller active space such as (10,10) has been used and reasonable results have been obtained.[50] Therefore, in order to find a well-balanced active space, we explored active spaces smaller than (12,12).

We found that the calculated CASSCF dipole moments of S_0, S_1, and S_2 depend strongly on the choice of the active space; this indicates that the choice of active space has a big impact on the charge distribution, *i.e.*, on the density. For example, for S_2 of **11c-dimethyl**, a CASSCF calculation using the (10,10) active space (#1 in Table 2) gives a dipole moment of 9.60 debye (D), while that using the (12,12) active space gives 23.22 D (Table 2). This difference can be explained by different active spaces converging to different wave functions (Table 3; Tables S8 and S9 of the ESI†).

As one way to characterize the wave functions, we evaluated the multireference character of each root by calculating its M diagnostic[51] values (Table 3). The M diagnostic value is a measure of how far the state deviates from a single-configuration ideal (and for excited states, from the single-configuration, single-excitation ideal). By our usual definition where the multireference character is small if $M < 0.05$, modest if $0.05 \leq M \leq 0.10$, and large if $M > 0.10$, most of these roots have large multireference character, and S_2 has an especially high multireference character. Comparing M values and dipole moments across active spaces, we find that the dipole moment difference between active spaces correlates with the difference in their M values. This is reasonable because similar wave functions are expected to have similar M values and similar dipole moments.

The dipole moment is an attractive candidate for evaluating the balance of various active space choices because the dipole moment is in principle a physical observable. It is the first moment of density, and thus the quality of the predicted dipole moment is an indication of the quality of the predicted density, which is determined by the wave function.

To investigate the possibility of reducing the dramatic difference in dipole moments, for each active space, we did a few CASSCF calculations with different guess orbitals. The CASSCF(10,10) calculation starting from CASSCF(12,12) orbitals

Table 3 The dominant configurations, the weight of each dominant configuration, and the M diagnostic value(s) of each root from CASSCF/TZVP calculations using different active spaces. The solution for the CASSCF(10,10) calculation using CASSCF(8,8) or HF orbitals as the guess orbitals is labeled #1, and the solution for the CASSCF(10,10) calculation using CASSCF(12,12) orbitals as the guess orbitals is labeled #2

	S_0			S_1			S_2		
	Dominant configurations[a]	Weight (%)	M^b	Dominant configurations[a]	Weight (%)	M^b	Dominant configurations[a]	Weight (%)	M^b
(4,4)	2200	92.1	0.09	2ud0	77.7	0.50	2020	35.0	0.46
							u2d0	29.6	
(6,6)	222000	91.4	0.08	22ud00	80.2	0.38	2u2d00	35.2	0.50
							220200	31.0	
							22u0d0	10.0	
(8,8)	22220000	80.3	0.12	222ud000	68.6	0.16	22202000	32.4	0.48
							22u2d000	27.7	
(10,10) #1	2222200000	83.2	0.11	2222ud0000	71.8	0.35	222u2d0000	33.4	0.47
							2222020000	28.3	
(10,10) #2	2222200000	83.9	0.12	2222ud0000	70.5	0.20	222u2d0000	43.1	0.54
							2222020000	19.7	
(12,12)	222222000000	68.2	0.16	22222ud00000	53.2	0.34	222220200000	28.7	0.53
				222222000000	11.2		2222u2d00000	19.5	
							22222u0d0000	10.8	

[a] Configurations that have a weight (square of the configuration interaction (CI)-coefficient) no less than 10% are considered dominant configurations. Each digit or letter in the configuration shows the occupation of the corresponding natural orbital: 2 means doubly-occupied, 0 means unoccupied, u means singly-occupied with a spin-up electron, and d means singly occupied with a spin-down electron. The order of the orbitals is the same as that in Tables S8 and S9 of the ESI. [b] The M diagnostic values are calculated based on the definition in Tishchenko *et al.*[51]

as the guess orbitals yielded a different set of wave functions (labeled #2) from the calculation using HF orbitals as guess orbitals (#1), as shown in Table 3 as well as Tables S8 and S9 of the ESI.† The total CASSCF energy of #2 is only 0.04 eV lower than #1. Note that, although CASSCF is variational for a certain active space, the variational principle does not suggest that a solution with a lower energy is always closer to the true solution. In contrast, using CASSCF(8,8) orbitals as guess orbitals yielded the same solution for CASSCF(10,10) as using HF orbitals as guess orbitals. For the (12,12) active space, starting from the CASSCF(10,10) orbitals (either #1 or #2) and HF orbitals gave the same solution. These results suggest that the large active-space dependence of the solutions is not likely due to convergence issues. Since none of the solutions obtained by these further variations were able to eliminate the large differences between dipole moments, it is unlikely that the large differences in dipole moments between active spaces are artifacts from guess orbitals.

Since the dipole moment can serve as a simplified descriptor for the differences in wave functions, we decided to select an active space based on the quality of the dipole moments it predicts. To assess this quality, we first need to calculate reasonably trustworthy dipole moments by some other method.

A previous study by Jacquemin[52] shows TDDFT might underestimate the lowest-excited-state dipole moments, but by only 1.0–1.5 D on average compared to the resolution-of-identity second-order approximate coupled cluster (RI-CC2) method for molecules that are about the size of retinal and have states with strong CT character. The same study also shows that KS-DFT tends to overestimate the ground state dipole moment by 0.15–0.30 D in mean absolute error (MAE), with the exception of M06-HF[53] whose largest error is 0.98 D (we shall see that this is consistent with our finding that M06-HF has the largest ground-state dipole moment among the functionals we considered).

In order to explore what might be reasonable for the dipole moments, we calculated dipole moments of the first three singlet states of retinal by KS-DFT and TDDFT using a diverse set of density functionals. We considered the hybrid functionals M06-2X (54% HF exchange),[26] M06-HF (100% HF exchange),[53] CAM-B3LYP (19% HF exchange in the short-interelectronic-distance limit and 65% in the long-range limit),[54] and PBE0 (25% HF exchange).[55,56] The latter two are hybrid functionals with the generalized gradient approximations (GGA), and the former two are hybrid meta-GGA functionals. These functionals have been demonstrated to predict the ground state dipole moments for both single-reference and multireference systems within 0.51 D (0.96 D for M06-HF) MAE of experimental values.[57] As shown in Table 2, although the density functionals considered are quite different from each other, they give dipole moments consistent with each other. We see that the variations of dipole moments among the various active spaces are significantly greater than the errors TDDFT may introduce, and we see that the (10,10) active space #1 of Table 2 is the only active space whose dipole moments fall within the range of errors of TDDFT. In particular, for ground-state dipole moments, which KS-DFT can predict reasonably well, the prediction for the (12,12) active space is 7.67 D greater than that for solution #1 of the (10,10) active space, 5.77 D greater than that for solution #2 of the (10,10) active space, and 5.42 D greater than that predicted by M06-HF. This is a strong indication that the (12,12) active space is not as good as the (10,10) active space for **11c-dimethyl**. Solution #2 of the (10,10) active space not only

differs from solution #1 of the same active space in dipole moments, but it also differs greatly from CASSCF(12,12) and CASSCF(10,10) #1 for the composition of dominant configurations (Table 3), natural orbital occupations (Table S8 of the ESI†), vertical excitation energies, and oscillator strengths (Table S2 of the ESI†). Based on dipole moments, we choose (10,10) as the active space for both **11c** and **11t**, and we choose solution #1, which is from CASSCF(10,10) calculations, using CASSCF(8,8) or HF orbitals as the guess orbitals.

In the following discussions, we focus on solution #1 for CASSCF(10,10)/TZVP.

3.2. Basis set effects and vertical excitation energies

To evaluate the effect of basis set on dipole moments and vertical excitation energies, in addition to TZVP,[34,35] we also tested def2-SVP,[36,37] def2-SVPD,[36–38] def2-TZVP,[36,37] ma-SVP,[39] and ma-TZVP.[39] The results are reported in Tables S1 and S2 of the ESI.† In principle, the addition of diffuse functions, such as those in def2-SVPD, ma-SVP and ma-TZVP, may result in a more accurately calculated dipole moment. However, for CASSCF, different basis sets may cause the wave function to converge to a different set of solutions (*i.e.* different configurations for each state), similar to the effect of active spaces as we have discussed in the previous section, and thus dipole moments from different basis sets may not be directly comparable. However, we do not observe a considerable impact of basis set on the dipole moments and vertical excitation energies from TDDFT calculations, and certainly we see less impact than the choices of density functionals. For **11c-dimethyl**, the greatest standard deviation of TDDFT dipole moments of each state among the states concerned is only 0.11 D (M06-2X and S_2) or 0.21 D (M06-HF and S_0). The standard deviation of TDDFT vertical excitation energy for any transition concerned is no more than 0.03 eV for a given density functional. However, for the same active space, the standard deviation of CASSCF dipole moments calculated based on Table S1 of the ESI† can be 3.03 D for the ground state, and as large as 7.86 D for the second excited state (the greatest among all excited states concerned).

The big difference in CASSCF dipole moments caused by basis set is a clear indication that different basis sets caused the calculation to converge to different solutions, which is reflected in vertical excitation energies (Tables S1 and S2 of the ESI†). For example, for **11c-dimethyl**, the CASSCF(10,10) dipole moments of S_0, S_1, and S_2 are 16.45 D, 10.75 D, and 9.60 D for TZVP, 16.46 D, 10.76 D, and 9.60 D for ma-SVP, and 21.83 D, 5.96 D, and 21.00 D for def2-TZVP (Table S1 of the ESI†). This suggests that ma-SVP is more likely to give similar results to TZVP than def2-TZVP is to TZVP. Indeed, the CASSCF(10,10) vertical excitation energies of $S_0 \rightarrow S_1$ and $S_0 \rightarrow S_2$ are 2.61 eV and 3.71 eV for TZVP, 2.62 eV and 3.71 eV for ma-SVP, and 3.20 eV and 3.81 eV for def2-TZVP (Table S2 of the ESI†). The vertical excitation energy differences between different basis sets are generally decreased at the CASPT2, MS-CASPT2, and MC-PDFT levels, but they still exhibit a correlation with the dipole moments. For example, the $S_0 \rightarrow S_1$ vertical excitation energy for TZVP is greater than def2-TZVP by 0.08 eV (CASPT2) or 0.26 eV (tPBE), but it only differs with ma-SVP by 0.01 eV (CASPT2 or tPBE). In general, MC-PDFT vertical excitation energies are more sensitive to the wave functions than CASPT2 or MS-CASPT2, and they show larger differences than CASPT2 or MS-CASPT2 when CASSCF dipole moments differ greatly from TDDFT dipole moments.

Since CASSCF(10,10)/TZVP gives **11c-dimethyl** dipole moments similar to TDDFT, and TZVP has only seventy percent of the number of basis functions of def2-TZVP, we decided to use the basis set TZVP and the active space selection discussed earlier. Because **11t-butyl** is chemically similar to **11c-dimethyl**, we used TZVP for **11t-butyl** too.

With these selections, we calculated the spectra and found that for both **11c-dimethyl** and **11t-butyl**, the first two excited states are both chain-to-chain ($\pi \rightarrow \pi^*$) transitions for both CASSCF and TDDFT. For these two excited states (for **11c-methyl**), the spatial overlaps[58] between B3LYP orbitals involved in the excitations are 0.68 and 0.72, respectively,[59] which means the spatial overlaps between the orbitals are relatively large. In addition, the summation of the change in charge centroid and the change of the variance of the charge centroid calculated with PBE0 gives 1.9 Å and 2.4 Å for these states (**11c-butyl**), respectively, which implies the charge transfer characters of these excitations are short-range in nature.[60] The characters of these states of the most stable three conformations of **11c-dimethyl** calculated with CASSCF(10,10)/TZVP in this study are consistent with these results and are shown in Table S6 of the ESI.† Table 4 compares the vertical excitation energies of **11c-dimethyl** and **11t-butyl** to one another and to previous calculations.[61] We see differences of 0.2–0.4 eV between CASPT2 and tPBE (and differences of 0.3–0.5 eV between MS-CASPT2 and tPBE). Since there is no experiment that directly gives the vertical excitation energies, we must compare to the experimental spectra to determine which method is more accurate. We turn next to that comparison.

Table 4 Vertical excitation energies (in eV) and oscillator strengths (in parentheses) of **11c-dimethyl** and **11t-butyl** using various methods

	CASSCF	CASPT2	MS-CASPT2	MC-PDFT/tPBE	M06-2X	RI-CC2/def-TZVP[a]	M06-HF
11c							
S_1	2.61	2.37 (1.51)	2.50	2.01 (1.28)	2.44 (1.45)	2.10 (1.47)	2.59 (1.66)
S_2	3.71	3.42 (0.14)	3.50	3.21 (0.14)	3.56 (0.40)	3.30 (0.26)	4.10 (0.23)
11t							
S_1	2.63	2.38 (1.76)	2.50	1.97 (1.46)	2.45 (1.78)	—	2.60 (2.01)
S_2	3.69	3.42 (0.16)	3.50	3.21 (0.15)	3.57 (0.42)	—	4.12 (0.17)

[a] Calculations from Zaari *et al.*[61]

3.3. Absorption spectra, including conformational averaging

Nielsen *et al.*[25] measured the absorption spectra of **11c-dimethyl** and **11t-butyl** *in vacuo* at room temperature. They found broad, somewhat structured peaks for S_1 and a narrower peak for S_2. Prior to that, the same group (Andersen *et al.*[62]) reported a similar spectrum for **11t-butyl,** which was the first measurement of the absorption spectrum of the protonated Schiff-base retinal *in vacuo*. Rajput *et al.*[63] measured the photodissociation spectra of **11c-butyl** and found a plateau from 530 nm to 610 nm instead of the peaks seen in Nielsen *et al.*'s photodissociation measurement. Theoretical studies have been carried out by several groups to explain the broad band. The most recent such study was carried out by Valsson and Filippi,[27] and they found that neither CASPT2 nor second-order *n*-electron valence-state perturbation theory (NEVPT2) gave excitation energies with sufficient variation between conformations (considering only the three lowest-energy conformations) to explain the photodissociation experiments; they concluded that the photodissociation spectrum is not indicative of the absorption spectra. More recently, Coughlan *et al.*[64] measured the photoisomerization action spectra of **11t-butyl** and its isomers/photoisomers attempting to resolve the controversy, and obtained spectra that do not have the plateau and that resemble those earlier spectra by Andersen *et al.*[62] and Nielsen *et al.*[25] Therefore, we compare to the spectra obtained by Nielsen *et al.*[25] and Coughlan *et al.*[64] instead of that by Rajput *et al.*[63] Because contaminations from different photoisomers cannot be ruled out from the spectra obtained by Coughlan *et al.* (*e.g.* the **11t-butyl** band may contain a small contribution of **13c-butyl**, and the **11c-butyl** band may be assigned to **9c-butyl** instead), and the laser source used did not include wavelengths below 410 nm to fully characterize the $S_0 \rightarrow S_2$ band, we mainly compare to the spectra by Nielsen *et al.*

The retinal molecule has many torsional degrees of freedom. To calculate spectra that can be compared to experiment, we must average over the low-energy conformations. It has been recognized in a number of theoretical[27–29,65,66] and experimental[63,67] studies that the rotation of the β-ionone ring and torsions around the single bonds on the chain may result in multiple low-energy structures; however, most studies focus on the rotation of the β-ionone ring, and there has not been a systematic study on all major torsional degrees of freedom in retinal except for Coughlan *et al.* in an attempt to predict the mobilities of different isomers.[64] However, Coughlan *et al.* assumed that there were only three possibilities for the torsion describing the rotation of the β-ionone ring. Therefore, we scanned the dihedral angles of **11c-dimethyl** with a finer grid defined in Table 1 to find low energy conformations. The conformations within 3 kcal mol^{-1} of the lowest-energy conformation are summarized in Table 5. For **11t-butyl**, for simplicity we only considered the conformations that correspond to the three most populated conformations of **11c-dimethyl**, and these conformations are summarized in Table 6.

The spectrum of each conformation and the averaged spectra generated with *FCBand* are compared to the experimental absorption spectra of Nielsen *et al.*[25] in Fig. 2 and of both Nielsen *et al.*[25] and Coughlan *et al.*[64] in Fig. 3, and the peak positions are compared in Table 7. Because the spectrum of Coughlan *et al.*[64] assigned to **11c-butyl** has a worse signal-to-noise ratio than the spectrum of the *trans*-isomer, and it can also be assigned to **9c-butyl**, we choose not to compare it with our **11c-dimethyl** spectrum. From Fig. 2, 3 and Table 7, we see that, although the experimental plateau from Rajput *et al.*[63] is still not explained, the maximum-wavelength peak of each band from tPBE matches well with that from the experiments of Nielsen *et al.*[25] and Coughlan *et al.*,[64] and tPBE clearly outperforms CASPT2. Although Table S2 of the ESI† shows CASPT2(12,12) has the $S_0 \rightarrow S_1$ vertical excitation energy closer to experiment than CASPT2(10,10) by approximately 0.15 eV, the vertical excitation energy difference between CASPT2(12,12) and experiments is still greater than that between CAS(10,10)-PDFT (tPBE) and experiments.

The overestimation of the $S_0 \rightarrow S_1$ vertical excitation energy of CASPT2 and MS-CASPT2 is consistent with previous theoretical studies,[27,68] although in these studies no conformational averaging was carried out, and the geometry, active space, and basis set used are different from ours. In Granovsky's study,[68] using a PBE0/cc-pVDZ geometry of **11t-butyl** with θ_6 similar to s0048, a calculation by extended multi-configuration quasi-degenerate second-order perturbation theory (XMCQDPT2) based on an SA(2)-CASSCF(12,12) reference function is reported to give a 593 nm (2.09 eV) vertical excitation energy for $S_0 \rightarrow S_1$, which is slightly worse than our SA(3)-CAS(10,10)-PDFT (tPBE) results (Tables 4 and 7). Furthermore, the PDFT post-SCF calculations are faster than the PT2 post-SCF calculations by a factor of $\sim$30 for examples in our study.

Comparing Table 4 with Table 7, it seems that averaging over various conformers made the simulated spectra differ slightly more from experimental spectra than the unaveraged ones of the lowest-energy conformer (s0048). However, we still need to take different conformers into consideration. While some conformers contribute

Table 5 Conformations of **11c-dimethyl** within 3 kcal mol^{-1} of the lowest-energy conformation. The label for each conformation is randomly assigned by the *MSTor* program in the present study. The percentage of each conformation as calculated from the Gibbs free energy at 298.15 K is also shown. Relative energies (E) are in kcal mol^{-1}. Torsional angles θ (in degrees) are defined in Table 1

Rank	Label	Relative E	%	θ_6	θ_8	θ_{10}	θ_{12}	θ_{14}
1	s0048	0.00	36.4	−40	178	179	179	180
2	s0096	0.37	22.3	−170	−180	180	180	180
3	s0144	0.38	30.1	44	−178	−179	−179	−180
4	s0003	1.69	3.6	−41	177	176	−22	177
5	s0110	1.98	1.7	−170	179	177	−20	177
6	s0134	2.25	1.8	45	−180	177	−22	178
7	s0042	2.50	2.6	−38	−25	−179	180	180
8	s0126	2.89	1.5	42	26	180	−179	−180

Table 6 The three most stable conformations of **11t-butyl**. The percentage of each conformation calculated from the Gibbs free energy at 298.15 K is also shown. Relative energies (E) are in kcal mol^{-1}. Torsional angles θ (in degrees) are defined in Table 1

Rank	Label	Relative E	%	θ_6	θ_8	θ_{10}	θ_{12}	θ_{14}
1	s0048	0.00	53.8	−40	178	180	180	180
2	s0144	0.36	25.9	44	−178	−180	−180	180
3	s0096	0.40	20.2	−170	−180	180	180	179

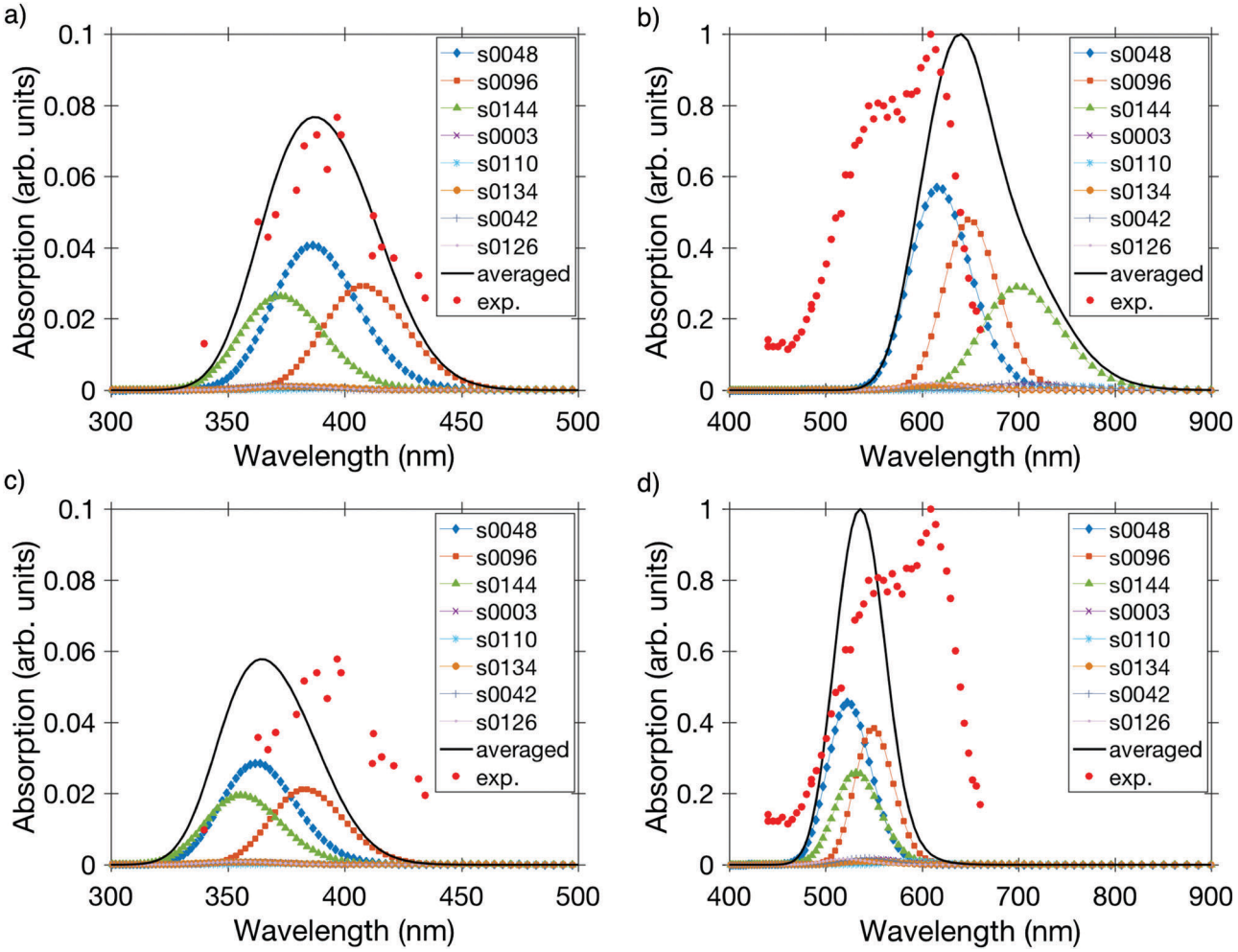

Fig. 2 Simulated spectra of **11c-dimethyl** from (a and b) MC-PDFT with tPBE and (c and d) CASPT2. Subplots (a) and (c) show the simulations of the short-wavelength $S_0 \rightarrow S_2$ band, and subplots (b) and (d) show the simulations of the long-wavelength $S_0 \rightarrow S_1$ band. For the simulations, thermal distributions are calculated at 298.15 K. The simulated band of each isomer is weighted by its population, and the averaged band is the average of these population-weighted bands. The averaged simulated spectrum and the experimental spectrum are scaled such that the maximal absorption of the $S_0 \rightarrow S_1$ peak is 1.0. Red dots are experimental (exp.) spectra from Nielsen *et al.*[25] Because the experiment was carried out with two different laser sources, the intensities below and above 435 nm are not on the same scale; therefore, we normalized the experimental results below 435 nm to the theoretical short-wavelength peak in each of the plots (a) and (c), and the experimental results above 435 nm to the theoretical long-wavelength peak in each of the plots (b) and (d). In these plots, all conformations other than s0048, s0096, and s0144 have absorption close to zero.

to shifting the maximum absorption peak of the spectrum away from the experimental maximum absorption peak, they explain the broadening of the band (Fig. 2 and 3). In addition, as temperature changes, the distribution of the conformers changes, which in turn changes the shape and the location of the band, as explained below.

At room temperature, the three lowest-energy conformations mainly differ only in θ_6, which governs the rotation of the β-ionone ring. However, the populations of other conformations, especially those with θ_8 deviating from 180°, start to approach these three conformations as temperature increases (Table S4 of the ESI†). As shown in the simulated spectra in Fig. S2–S5 of the ESI† and in Fig. 2 and 3, conformational averaging affects both the MC-PDFT spectrum and the CASPT2 spectrum. Furthermore, as shown in Table S6 of the ESI,† conformational changes also affect the characters of the wave functions. The tPBE vertical excitation energies from different conformations have a greater variance than those calculated by CASPT2, and they explain the broadening of the $S_0 \rightarrow S_1$ band better than CASPT2 (Table S7 of the ESI†). Interestingly, the ratios between the weights of the conformations s0096 and s0048 and between the weights of the conformations s0144 and s0048 both increase as temperature increases (Tables S4 and S5 of the ESI†), making the band red-shift slightly as temperature increases. This red shift is not significant for the averaged tPBE spectra likely because of the relatively low tPBE oscillator strength of s0144 associated with the low vertical excitation energy of this conformation.

From Tables 5 and 6, it might seem that the conformations of s0048 and s0144 are nearly mirror images of each other,

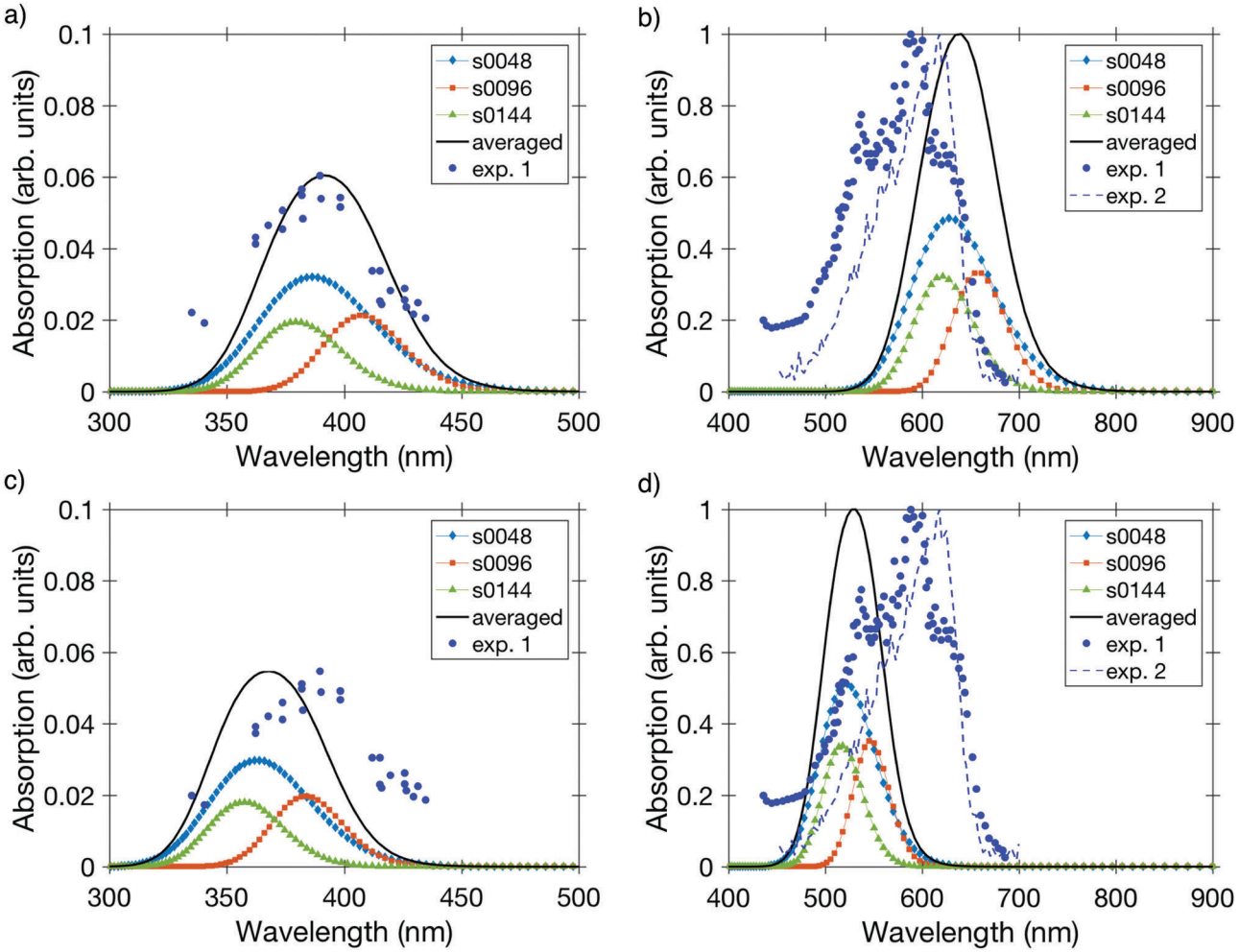

Fig. 3 Simulated spectra of **11t-butyl** from (a and b) MC-PDFT with tPBE and (c and d) CASPT2. Subplots (a) and (c) show the simulations of the short-wavelength $S_0 \rightarrow S_2$ band, and subplots (b) and (d) show the simulations of the long-wavelength $S_0 \rightarrow S_1$ band. For the simulations, thermal distributions are calculated at 298.15 K. The simulated band of each isomer is weighted by its population, and the averaged band is the average of these population-weighted bands. The averaged simulated spectrum and the experimental spectrum are scaled such that the maximal absorption of the $S_0 \rightarrow S_1$ peak is 1.0. Blue dots represent the experimental spectrum from Nielsen *et al.*[25] (exp. 1), and blue dash lines represent the experimental spectrum from Coughlan *et al.*[64] (exp. 2). Because the experiment by Nielsen *et al.*[25] was carried out with two different laser sources, the intensities below and above 435 nm are not on the same scale; therefore, we normalized the experimental results below 435 nm to the theoretical short-wavelength peak in each of the plots (a) and (c) and the experimental results above 435 nm to the theoretical long-wavelength peak in each of the plots (b) and (d). For the spectrum by Coughlan *et al.*,[64] the band below 450 nm is assigned to $S_0 \rightarrow S_2$ and thus it is not shown in (b) and (d). It is very weak and it does not include signals below 410 nm, so we chose not to compare it with our $S_0 \rightarrow S_2$ band in (a) and (c).

which would make it hard to explain the differences in their absorption spectra. However, this is not true. The retinal molecule does not have a plane of reflection even when the torsional angle θ_6 is 0 because of the puckering of the β-ionone ring.

Analysis of the Franck–Condon active modes helps to understand the differences between the spectra of different conformers, and here we provide such an analysis for **11c-dimethyl** (Table 8). Under the FC-DHO approximation, the line shape of an excitation is a Gaussian function centered at the vertical excitation energy, with a half width at half maximum of

$$W = \sqrt{(\ln 2)D^2} \tag{1}$$

with

$$D^2 = \sum_j d_j^2 \tag{2}$$

where

$$d_j = |\Delta_j \omega_j| \tag{3}$$

and the sum runs over all normal modes j, ω_j is the frequency of the ground-electronic-state vibrational mode j, W, D, d_j, and ω_j are expressed in the same energy units (in the present discussion, we use cm^{-1}), and Δ_j is the displacement of dimensionless normal coordinate j from the ground-state equilibrium geometry to the excited-state equilibrium geometry; Δ_j is approximated in terms of ω_j and the gradient of the excited-state potential energy with

Table 7 Peak positions (wavelength in nm and excitation energy in eV) of the experimental bands and the averaged simulated bands in the 298.15 K spectra of **11c-dimethyl** in Fig. 2 and **11t-butyl** in Fig. 3. For comparison, the peak positions in the absorption spectra assigned to **11c-butyl** (and/or other *cis* isomers) and **11t-butyl** in the experiment at 314 K by Coughlan *et al.* are also included. Note that Nielsen *et al.*[25] assigned the longest-wavelength peak instead of the maximum-absorption peak of their $S_0 \rightarrow S_1$ band as the S_1 band origin

Molecule	Method	λ S_1	ΔE S_1	λ S_2	ΔE S_2
11c-dimethyl	Exp.[a]	610	2.03	390	3.18
	Exp. (**11c-butyl** and/or other *cis* isomers)[b]	615 ± 10	2.02 ± 0.03	—	—
	CASPT2	536	2.31	364	3.41
	MC-PDFT/tPBE	641	1.93	386	3.21
11t-butyl	Exp.[a]	620	2.00	385	3.22
	Exp.[b]	618 ± 5	2.01 ± 0.02	—	—
	CASPT2	531	2.33	370	3.35
	MC-PDFT/tPBE	641	1.93	391	3.17

[a] Nielsen *et al.*[25] [b] Coughlan *et al.*[64]

respect to nuclear coordinates at the ground-state equilibrium geometry. The percentage contribution of mode j to the width is

$$P_j = d_j^2/D^2 \times 100\% \quad (4)$$

and in the cases examined, we found that the sum of the three largest P_j values $P_{j_1} + P_{j_2} + P_{j_3}$ is in the range 37–47% with none of the other modes contributing more than 7% to the width. Table 8 shows j, ω_j, the nature of the mode, d_j, and P_j for the three modes that contribute the most to each of the transitions $S_0 \rightarrow S_1$ and $S_0 \rightarrow S_2$ for conformations s0048, s0096, and s0144. The ESI† gives j, ω_j, and d_j for the other modes for these transitions. Although **11c-dimethyl** has 165 vibrational modes, 75% of the contribution to the width comes from the 15–23 most active modes, depending on the conformation and the excitation.

3.4. Effect of terminal groups on vertical excitation energy

Although we focus in this study on **11c-dimethyl** and **11t-butyl** in order to compare with experiments, various other research groups have been studying retinals with other terminal groups. Therefore, we looked into the vertical excitation energies of **11t** with some other terminal groups, and the results are shown in Table 9. The table shows that the $S_0 \rightarrow S_2$ transition energies are less sensitive to terminal groups than are the $S_0 \rightarrow S_1$ transition energies. Furthermore, for the $S_0 \rightarrow S_1$ transition, tPBE transition energies are more sensitive to the terminal group than are those calculated by CASPT2 or MS-CASPT2. Nevertheless, similar to CASPT2 and MS-CASPT2, the tPBE vertical excitation energies for the $S_0 \rightarrow S_1$ transition are in the order of **11t-butyl** > **11t-dimethyl** > **11t-methyl**.

Some of the details of the conformational dependences are quite remarkable. Consider, for example, conformations s0048 and s0144. For both conformations, at the CASSCF level, the $S_0 \rightarrow S_1$ excitation energy is the lowest for butyl, whereas with CASPT2 and MS-CASPT2, it is highest for butyl. Encouragingly, the tPBE results show the same trend as CASPT2 and MS-CASPT2 for both conformations, which suggests that this trend is likely to be reliable. This result implies that the effect of terminal groups should not be ignored in future studies of retinal, and tuning the terminal groups of retinal, which may involve introducing an unnatural amino acid into the opsin protein, may be one other way to tune the absorption spectrum of the photoreceptor.

Table 8 Dominant Franck–Condon active modes for the first two excitations of **11c-dimethyl** conformers[a]

j	ω_j	Mode[b]	d_j	P_j (%)
s0048, S_1				
37	1672	C5═C6, C7═C8 sym str	600	27
40	1567	C11═C12 str	344	9
36	1707	C5═C6, C7═C8 asym str	311	7
s0096, S_1				
36	1672	C7═C8 str	356	14
38	1630	C9═C10, C12–C13 (sym), C13═C14 (asym) str	323	12
37	1660	C5═C6 str	316	11
s0144, S_1				
37	1677	C5═C6, C7═C8 sym str	602	27
36	1709	C5═C6, C15═N sym str	393	12
40	1569	C11═C12 str	344	9
s0048, S_2				
36	1707	C5═C6, C7═C8 asym str	944	30
40	1567	C11═C12 str	384	5
100	1015	C17 CH_3 rock	344	4
s0096, S_2				
36	1672	C7═C8 str	677	20
37	1660	C5═C6 str	677	20
77	1289	C8,C10,C11,C12,C14,C15 CH in-plane bend	365	6
s0144, S_2				
36	1709	C5═C6, C15═N (sym), C7═C8 (asym) str	933	28
40	1569	C11═C12 str	386	5
146	254	C8 out-of-plane bend	378	5

[a] j = mode number (modes numbered in order of decreasing frequency); ω_j = frequency in cm^{-1}; d_j = frequency-weighted displacement in cm^{-1}; P_j = percentage contribution to width. Note that mode j for one conformer is not necessarily the same as mode j for another. [b] sym = symmetric; asym = asymmetric; str = stretch. Only the heavy atoms involved in the dominant motion are listed, unless a C–H motion is dominant.

Table 9 Vertical excitation energies and oscillator strengths of **11t** with various terminal groups and conformations

			Excitation energy (eV)				Osc. str.	
Transition	Molecule	Conf.[a]	CASSCF	CASPT2	MS-CASPT2	MC-PDFT/tPBE	CASPT2	MC-PDFT/tPBE
$S_0 \rightarrow S_1$	**11t-butyl**	s0048	2.63	2.38	2.50	1.97	1.76	1.46
		s0096	2.54	2.27	2.38	1.89	1.90	1.58
		s0144	2.65	2.40	2.53	2.00	1.77	1.47
	11t-dimethyl	s0048	3.18	2.31	2.42	1.72	1.15	0.86
		s0096	2.54	2.26	2.37	1.88	1.91	1.59
		s0144	3.21	2.34	2.45	1.74	1.16	0.87
	11t-methyl	s0048	3.09	2.28	2.42	1.69	1.20	0.89
		s0096	2.86	2.17	2.35	1.64	1.40	1.06
		s0144	3.13	2.31	2.45	1.72	1.21	0.90
$S_0 \rightarrow S_2$	**11t-butyl**	s0048	3.69	3.42	3.50	3.21	0.16	0.15
		s0096	3.43	3.23	3.31	3.04	0.17	0.16
		s0144	3.74	3.47	3.55	3.27	0.15	0.14
	11t-dimethyl	s0048	3.82	3.44	3.63	3.24	0.14	0.13
		s0096	3.44	3.24	3.31	3.04	0.16	0.15
		s0144	3.86	3.49	3.67	3.30	0.14	0.13
	11t-methyl	s0048	3.77	3.41	3.58	3.20	0.13	0.12
		s0096	3.52	3.22	3.38	3.00	0.11	0.10
		s0144	3.82	3.47	3.63	3.27	0.12	0.11

[a] Each conformation has roughly the same torsional angles as conformations with the same label in Table 6.

4. Conclusions

In this study, we used MC-PDFT for describing electronic excitations in retinal. We presented a strategy to select the active space of CASSCF calculations based on a simple characterization of the wave functions, namely the ground- and excited-state dipole moments. We also evaluated the effect of basis set sizes on dipole moments, vertical excitation energies, and oscillator strengths in CASSCF, CASPT2, MS-CASPT2, MC-PDFT, and TDDFT calculations. While basis sets do not have a significant impact on TDDFT results, they do change the reference wave functions in some cases. Nevertheless, we were still able to decide basis sets based on dipole moments. The selection of the active space and basis set is often difficult in multiconfiguration calculations, and our strategy based on dipole moments provided a systematic and effective way to make this selection for the present problem.

To our knowledge, the present study is the most systematic scanning of retinal conformations for considering thermal distributions in simulating the retinal spectra. And we have shown that it is necessary to consider more conformations, including all local minima from rotating the β-ionone ring, to simulate the broadening of the spectra. Carrying out the conformational averaging, we find that MC-PDFT gives a broader distribution of excitation energies than CASPT2 for the same set of retinal conformations, and it reproduces the absorption spectra of **11c** and **11t** better than CASPT2 in both the broadening and the location of the band.

The retinal excitations are important not only just in their own right but also because they serve as prototypes for excitations with significant charge transfer character. We found that MC-PDFT provides an efficient and accurate way to study retinal excitations and that it is more accurate than CASPT2 when compared to experimental absorption spectra, which is encouraging because it is at least one order of magnitude faster than CASPT2. In addition, an MC-PDFT calculation does not involve parameters such as the imaginary shift or IPEA shift used in CASPT2. This demonstrates that it is a powerful new tool to study and design systems involving charge-transfer excitations that are too large in size for multireference perturbation theory methods, such as larger chromophores and organic semiconductors that are important in biological and energy applications.

Conflicts of interest

There are no conflicts to declare.

Acknowledgements

This work was supported in part by the Air Force Office of Scientific Research by grant no. FA9550-16-1-0134.

References

1 A. Altun, S. Yokoyama and K. Morokuma, *Photochem. Photobiol.*, 2008, **84**, 845–854.
2 L. M. Frutos, T. Andruniów, F. Santoro, N. Ferré and M. Olivucci, *Proc. Natl. Acad. Sci. U. S. A.*, 2007, **104**, 7764–7769.
3 K. Fujimoto, S. Hayashi, J.-Y. Hasegawa and H. Nakatsuji, *J. Chem. Theory Comput.*, 2007, **3**, 605–618.
4 R. González-Luque, M. Garavelli, F. Bernardi, M. Merchán, M. A. Robb and M. Olivucci, *Proc. Natl. Acad. Sci. U. S. A.*, 2000, **97**, 9379–9384.
5 C. A. Guido, D. Jacquemin, C. Adamo and B. Mennucci, *J. Phys. Chem. A*, 2010, **114**, 13402–13410.
6 S. Hayashi, E. Tajkhorshid and K. Schulten, *Biophys. J.*, 2009, **96**, 403–416.

7 B. Lasorne, G. A. Worth and M. A. Robb, *Wiley Interdiscip. Rev.: Comput. Mol. Sci.*, 2011, **1**, 460–475.
8 D. Polli, P. Altoè, O. Weingart, K. M. Spillane, C. Manzoni, D. Brida, G. Tomasello, G. Orlandi, P. Kukura and R. A. Mathies, *Nature*, 2010, **467**, 440.
9 R. Rajamani, Y. L. Lin and J. Gao, *J. Comput. Chem.*, 2011, **32**, 854–865.
10 I. Schapiro and F. Neese, *Comput. Theor. Chem.*, 2014, **1040**, 84–98.
11 I. Schapiro, M. N. Ryazantsev, L. M. Frutos, N. Ferré, R. Lindh and M. Olivucci, *J. Am. Chem. Soc.*, 2011, **133**, 3354–3364.
12 E. Tapavicza, I. Tavernelli and U. Rothlisberger, *Phys. Rev. Lett.*, 2007, **98**, 023001.
13 X. Xu, S. Gozem, M. Olivucci and D. G. Truhlar, *J. Phys. Chem. Lett.*, 2012, **4**, 253–258.
14 J. M. Berg, J. L. Tymoczko and L. Stryer, *Biochemistry*, W.H. Freeman, New York, 2002.
15 V. R. Kaila, R. Send and D. Sundholm, *J. Phys. Chem. B*, 2012, **116**, 2249–2258.
16 X. Zhou, D. Sundholm, T. A. Wesołowski and V. R. Kaila, *J. Am. Chem. Soc.*, 2014, **136**, 2723–2726.
17 F. Melaccio, N. Calimet, I. Schapiro, A. Valentini, M. Cecchini and M. Olivucci, *J. Phys. Chem. Lett.*, 2016, **7**, 2563–2567.
18 R. Li, J. Zheng and D. G. Truhlar, *Phys. Chem. Chem. Phys.*, 2010, **12**, 12697–12701.
19 K. Andersson, P. A. Malmqvist, B. O. Roos, A. J. Sadlej and K. Wolinski, *J. Phys. Chem.*, 1990, **94**, 5483–5488.
20 J. Finley, P.-Å. Malmqvist, B. O. Roos and L. Serrano-Andrés, *Chem. Phys. Lett.*, 1998, **288**, 299–306.
21 R. K. Carlson, G. Li Manni, A. L. Sonnenberger, D. G. Truhlar and L. Gagliardi, *J. Chem. Theory Comput.*, 2014, **11**, 82–90.
22 G. Li Manni, R. K. Carlson, S. Luo, D. Ma, J. Olsen, D. G. Truhlar and L. Gagliardi, *J. Chem. Theory Comput.*, 2014, **10**, 3669–3680.
23 E. Runge and E. K. Gross, *Phys. Rev. Lett.*, 1984, **52**, 997.
24 B. O. Roos, P. R. Taylor and P. E. Si, *Chem. Phys.*, 1980, **48**, 157–173.
25 I. B. Nielsen, L. Lammich and L. H. Andersen, *Phys. Rev. Lett.*, 2006, **96**, 018304.
26 Y. Zhao and D. G. Truhlar, *Theor. Chem. Acc.*, 2008, **120**, 215–241.
27 O. Valsson and C. Filippi, *J. Phys. Chem. Lett.*, 2012, **3**, 908–912.
28 S. Zhu, M. F. Brown and S. E. Feller, *J. Am. Chem. Soc.*, 2013, **135**, 9391–9398.
29 R. Send and D. Sundholm, *J. Phys. Chem. A*, 2007, **111**, 8766–8773.
30 M. J. Frisch, G. W. Trucks, H. B. Schlegel, G. E. Scuseria, M. A. Robb, J. R. Cheeseman, G. Scalmani, V. Barone, G. A. Petersson, H. Nakatsuji, X. Li, M. Caricato, A. Marenich, J. Bloino, B. G. Janesko, R. Gomperts, B. Mennucci, H. P. Hratchian, J. V. Ortiz, A. F. Izmaylov, J. L. Sonnenberg, D. Williams-Young, F. Ding, F. Lipparini, F. Egidi, J. Goings, B. Peng, A. Petrone, T. Henderson, D. Ranasinghe, V. G. Zakrzewski, J. Gao, N. Rega, G. Zheng, W. Liang, M. Hada, M. Ehara, K. Toyota, R. Fukuda, J. Hasegawa, M. Ishida, T. Nakajima, Y. Honda, O. Kitao, H. Nakai, T. Vreven, K. Throssell, J. A. Montgomery, Jr., J. E. Peralta, F. Ogliaro, M. Bearpark, J. J. Heyd, E. Brothers, K. N. Kudin, V. N. Staroverov, T. Keith, R. Kobayashi, J. Normand, K. Raghavachari, A. Rendell, J. C. Burant, S. S. Iyengar, J. Tomasi, M. Cossi, J. M. Millam, M. Klene, C. Adamo, R. Cammi, J. W. Ochterski, R. L. Martin, K. Morokuma, O. Farkas, J. B. Foresman and D. J. Fox, *Gaussian 09, Revision C.01*, Gaussian, Inc., Wallingford CT, 2010.
31 J. Zheng, R. Meana-Pañeda and D. G. Truhlar, *Comput. Phys. Commun.*, 2013, **184**, 2032–2033.
32 J. Zheng, S. L. Mielke, K. L. Clarkson and D. G. Truhlar, *Comput. Phys. Commun.*, 2012, **183**, 1803–1812.
33 F. Aquilante, J. Autschbach, R. K. Carlson, L. F. Chibotaru, M. G. Delcey, L. De Vico, N. Ferré, L. M. Frutos, L. Gagliardi and M. Garavelli, *J. Comput. Chem.*, 2016, **37**, 506–541.
34 A. Schäfer, H. Horn and R. Ahlrichs, *J. Chem. Phys.*, 1992, **97**, 2571–2577.
35 A. Schäfer, C. Huber and R. Ahlrichs, *J. Chem. Phys.*, 1994, **100**, 5829–5835.
36 F. Weigend, *Phys. Chem. Chem. Phys.*, 2006, **8**, 1057–1065.
37 F. Weigend and R. Ahlrichs, *Phys. Chem. Chem. Phys.*, 2005, **7**, 3297–3305.
38 D. Rappoport and F. Furche, *J. Chem. Phys.*, 2010, **133**, 134105.
39 J. Zheng, X. Xu and D. G. Truhlar, *Theor. Chem. Acc.*, 2011, **128**, 295–305.
40 J. P. Perdew, K. Burke and M. Ernzerhof, *Phys. Rev. Lett.*, 1996, **77**, 3865.
41 R. K. Carlson, D. G. Truhlar and L. Gagliardi, *J. Chem. Theory Comput.*, 2015, **11**, 4077–4085.
42 A. D. Becke, *Phys. Rev. A: At., Mol., Opt. Phys.*, 1988, **38**, 3098.
43 C. Lee, W. Yang and R. G. Parr, *Phys. Rev. B: Condens. Matter Mater. Phys.*, 1988, **37**, 785.
44 Y. Zhang and W. Yang, *Phys. Rev. Lett.*, 1998, **80**, 890.
45 P. Hohenberg and W. Kohn, *Phys. Rev.*, 1964, **136**, B864.
46 W. Kohn and L. J. Sham, *Phys. Rev.*, 1965, **140**, A1133.
47 U. von Barth and L. Hedin, *J. Phys. C: Solid State Phys.*, 1972, **5**, 1629.
48 S. L. Li and D. G. Truhlar, *J. Chem. Theory Comput.*, 2017, **13**, 2823–2830.
49 I. Alecu, J. Zheng, Y. Zhao and D. G. Truhlar, *J. Chem. Theory Comput.*, 2010, **6**, 2872–2887.
50 O. Weingart, P. Altoè, M. Stenta, A. Bottoni, G. Orlandi and M. Garavelli, *Phys. Chem. Chem. Phys.*, 2011, **13**, 3645–3648.
51 O. Tishchenko, J. Zheng and D. G. Truhlar, *J. Chem. Theory Comput.*, 2008, **4**, 1208–1219.
52 D. Jacquemin, *J. Chem. Theory Comput.*, 2016, **12**, 3993–4003.
53 Y. Zhao and D. G. Truhlar, *J. Phys. Chem. A*, 2006, **110**, 13126–13130.

54 T. Yanai, D. P. Tew and N. C. Handy, *Chem. Phys. Lett.*, 2004, **393**, 51–57.
55 C. Adamo and V. Barone, *J. Chem. Phys.*, 1999, **110**, 6158–6170.
56 J. P. Perdew, M. Ernzerhof and K. Burke, *J. Chem. Phys.*, 1996, **105**, 9982–9985.
57 P. Verma and D. G. Truhlar, *Phys. Chem. Chem. Phys.*, 2017, **19**, 12898–12912.
58 M. J. Peach, P. Benfield, T. Helgaker and D. J. Tozer, *J. Chem. Phys.*, 2008, **128**, 044118.
59 A. D. Dwyer and D. J. Tozer, *Phys. Chem. Chem. Phys.*, 2010, **12**, 2816–2818.
60 C. A. Guido, P. Cortona and C. Adamo, *J. Chem. Phys.*, 2014, **140**, 104101.
61 R. R. Zaari and S. Y. Wong, *Chem. Phys. Lett.*, 2009, **469**, 224–228.
62 L. H. Andersen, I. B. Nielsen, M. B. Kristensen, M. O. El Ghazaly, S. Haacke, M. B. Nielsen and M. Å. Petersen, *J. Am. Chem. Soc.*, 2005, **127**, 12347–12350.
63 J. Rajput, D. B. Rahbek, L. H. Andersen, A. Hirshfeld, M. Sheves, P. Altoè, G. Orlandi and M. Garavelli, *Angew. Chem., Int. Ed.*, 2010, **49**, 1790–1793.
64 N. Coughlan, B. Adamson, L. Gamon, K. Catani and E. Bieske, *Phys. Chem. Chem. Phys.*, 2015, **17**, 22623–22631.
65 B. Honig and M. Karplus, *Nature*, 1971, **229**, 558–560.
66 A. Cembran, R. González-Luque, P. Altoè, M. Merchán, F. Bernardi, M. Olivucci and M. Garavelli, *J. Phys. Chem. A*, 2005, **109**, 6597–6605.
67 Y. Toker, A. Svendsen, A. V. Bochenkova and L. H. Andersen, *Angew. Chem., Int. Ed.*, 2012, **51**, 8757–8761.
68 A. A. Granovsky, *J. Chem. Phys.*, 2011, **134**, 214113.

